*4838–4848* *Nucleic Acids Research, 2005, Vol. 33, No. 15*
*doi:10.1093/nar/gki795*

# Molecular details of quinolone–DNA interactions: solution structure of an unusually stable DNA duplex with covalently linked nalidixic acid residues and non-covalent complexes derived from it

**Karsten Siegmund[1], Shruti Maheshwary[2], Sukunath Narayanan[1], William Connors[2], Matthias Riedrich[2], Michael Printz[1] and Clemens Richert[1,2,*]**

[1]Institute for Organic Chemistry, University of Karlsruhe (TH), D-76131 Karlsruhe, Germany and [2]Department of Chemistry, University of Constance, D-78457-Konstanz, Germany

Received July 1, 2005; Revised and Accepted August 10, 2005

## ABSTRACT

**Quinolones are antibacterial drugs that are thought to bind preferentially to disturbed regions of DNA. They do not fall into the classical categories of intercalators, groove binders or electrostatic binders to the backbone. We solved the 3D structure of the DNA duplex (ACGCGU-NA)$_2$, where NA denotes a nalidixic acid residue covalently linked to the 2′-position of 2′-amino-2′-deoxyuridine, by NMR and restrained torsion angle molecular dynamics (MD). In the complex, the quinolones stack on G:C base pairs of the core tetramer and disrupt the terminal A:U base pair. The displaced dA residues can stack on the quinolones, while the uracil rings bind in the minor groove. The duplex-bridging interactions of the drugs and the contacts of the displaced nucleotides explain the high UV-melting temperature for *d*(ACGCGU-NA)$_2$ of up to 53°C. Further, non-covalently linked complexes between quinolones and DNA of the sequence ACGCGT can be generated via MD using constraints obtained for *d*(ACGCGU-NA)$_2$. This is demonstrated for unconjugated nalidixic acid and its 6-fluoro derivative. The well-ordered and tightly packed structures thus obtained are compatible with a published model for the quinolone–DNA complex in the active site of gyrases.**

## INTRODUCTION

Quinolones are heterocycles with a bicyclic core structure (**1**, Figure 1). They are known for their ability to inhibit bacterial topoisomerases (1). Quinolones have been used clinically for over 40 years, and some drugs from this class of compounds, such as levofloxacin and ciprofloxacin, are not only among the most frequently prescribed anti-infectives worldwide but also constitute the drug of choice against some life-threatening infections, including those by anthrax. Even mycobacterial infections can be treated with fluoroquinolones (2). Most clinically relevant quinolones contain a carboxylic acid function at position 3 and bulky substituents at one face of the bicyclic core, namely at positions 1 and 7 and/or 8, as shown schematically in structure **2**. Their aromatic core is smaller than that of typical intercalators, and their substituents are bulky enough to appear as protuberances from the plane of the aromatic ring, making it unlikely that they are part of an intercalated entity.

Though it is known that quinolones are active against topoisomerases of type II (gyrases) and type IV (3), the molecular

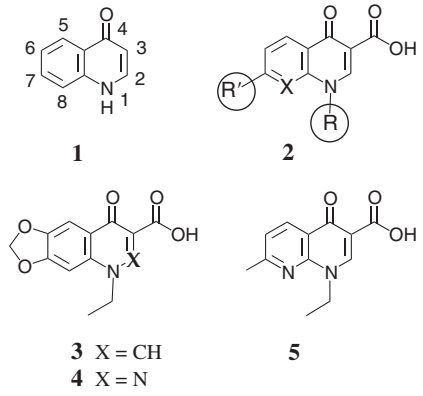


**Figure 1.** Structures of quinolones.

*To whom correspondence should be addressed. Tel: +49 721 608 2091; Fax: +49 721 608 4825; Email: cr@rrg.uka.de

details of their mode of action remain unclear. Gyrases cleave both strands of bacterial DNA, pass a double strand through the opening and re-ligate the cut ends to produce supercoils (4). The quinolones do not prevent the cleavage of the DNA but they interfere with the strand passage and re-ligation by stabilizing an intermediate of the catalytic cycle (5). If the enzyme falls off before the re-ligation of the DNA, double-strand breaks are introduced (6). Alternatively, the stabilization of an intermediate can arrest transcription or replication.

X-ray structures of gyrase subunits exist and detailed mechanisms for gyrase inhibition have been proposed (7–13), but no structure of a complex with substrate double-stranded DNA (dsDNA) and/or quinolones has been solved. Also, no high-resolution structures of quinolones non-covalently bound to DNA are available, though detailed physicochemical studies have shown affinity for dsDNA and single-stranded DNA (ssDNA) (14–16). It was concluded that quinolones bind to dsDNA in a mode that does not seem to be classical intercalation, classical groove binding or surface binding, but that the plane of the quinolone is near-perpendicular to the helical axis of the DNA (17). The distortion of the DNA induced by the gyrase is believed to favor binding of the drug to the nucleic acid. One model proposes cooperative binding of four quinolones to a bubble in dsDNA (18), whereas another proposes that two quinolones bind apart from each other and displace one nucleobase each in the DNA (19). In the ternary complex of quinolones, DNA and gyrase, fixation of the quinolones in space by chelation of the carboxyl group and the carbonyl group to a $Mg^{2+}$ ion that also coordinates to the DNA has been proposed previously (20). The two most popular models are qualitative, and precise coordinates for all components have not been generated.

Given the present inability to obtain high-resolution DNA–quinolone structures without the preorganizing effect of the gyrase (which in turn resists crystallization as a substrate–enzyme complex), preorganizing DNA and quinolones through covalent bonds that favor binding even for undisturbed DNA by ensuring a high local concentration of the ligand is perhaps worthwhile. There is evidence that tight and well-defined complexes can form in covalently linked hybrids. Nuclease selection assays employing synthetic libraries of acylated DNA strands revealed oxolinic acid (3) and cinoxacin (4) as duplex-stabilizing 5′-substituents (21–23). In addition, assays involving dynamic combinatorial libraries have identified nalidixic acid residues as substituents that stabilize duplexes with RNA targets (24,25). Nalidixic acid residues linked to ssDNA also enhance nuclease stability (26). Finally, the same residue stabilizes duplexes when linked to the 2′-position of a 2′-amino-2′-deoxyuridine residue at the 3′-terminal position of oligodeoxynucleotides (27).

For most covalently linked DNA–quinolone constructs, the details of the interaction between the nucleic acid and the drug have not yet been elucidated. One modeled structure for a complex involving two quinobenzoxaxines and two quinolones bound to DNA via complexation of four magnesium ions has been published previously (28), but the quinolones are extrahelical and have few contacts with the DNA. Also, a high-resolution structure has been obtained for a DNA duplex with 5′-appended oxolinic acid residues (29). The structure of the oxolinic acid–DNA complex with its disrupted T:A base pair is reminiscent of the model for non-covalent

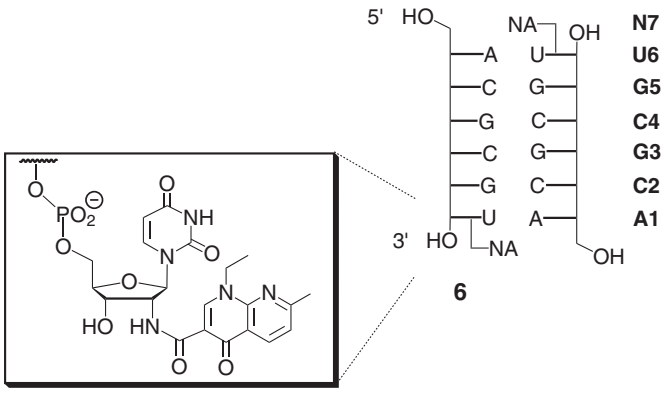


**Figure 2.** Structure of the duplex of compound **6**.

quinolone–DNA complexes proposed by Heddle *et al*. (30). The covalent link in this complex has led others to speculate (incorrectly) that a covalent link was also implied for the complex of quinolone, DNA and gyrases *in vivo* (31). Perhaps more importantly, attempts to model non-covalent quinolone–DNA complexes after this structure have been unsuccessful.

This prompted us to continue the search for stable and well-defined quinolone–DNA complexes, hoping to identify a more suitable one for modeling non-covalent complexes that are consistent with the structure–activity information available for quinolones. A covalently linked quinolone–DNA hybrid was recently identified that gives a melting temperature ($T_m$) much higher than that of the unmodified control duplex. This is the duplex $d$(ACGCGU-NA)$_2$ (**6**)$_2$ (Figure 2) (27). Its UV-melting temperature is up to 22°C higher than that of $d$(ACGCGT)$_2$. The hybrid has the quinolone attached to the 2′-position of a 3′-terminal residue. Here we present a high resolution structure of (**6**)$_2$, together with biophysical data on other quinolone–DNA constructs and two modeled non-covalent quinolone complexes, based on structural constraints for (**6**)$_2$.

## MATERIALS AND METHODS

### Synthesis

A sample of ACGCGU-NA (**6**) for NMR spectroscopy was synthesized following a route reported earlier (27) on a 6 μmol scale, using a Perseptive Biosystems 8909 Expedite DNA synthesizer, starting from controlled pore glass loaded with the quinolone-bearing nucleoside (27). Octamer $d$(CGGTTGAU-NA) (**7**) was prepared analogously, except that DNA synthesis of the unmodified portion was performed on a 1 μmol scale on an ABI 380 DNA synthesizer, following the manufacturer's recommendations. Nalidixic acid was obtained from Aldrich (Taufkirchen, Germany). The phosphoramidites used for the DNA syntheses were obtained from Proligo (Hamburg, Germany). MALDI-TOF spectra were recorded on Bruker BIFLEX III or REFLEX IV spectrometers in negative, linear mode, using a matrix mixture of 2,4,6-trihydroxyacetophenone (0.3 M in ethanol) and diammonium citrate (0.1 M in water) (2:1, v/v). Oligonucleotides were purified by high-performance liquid chromatography (HPLC) on a Macherey-Nagel Nucleosil C4 column

(250 mm × 4.6 mm), using a gradient of $CH_3CN$ (solvent B) in 0.1 M triethylammonium acetate, pH 7, and detection at 260 nm.

### *d*(ACGCGU-NA) (6)

Yield: 11%, as determined based on cpg loading; HPLC gradient: 0% B for 5 min to 25% B in 40 min, $Rt = 42$ min; MALDI-TOF MS $m/z$ for $C_{63}H_{84}N_{35}O_{36}P_5$ $[M–H]^-$: calcd 2007.8, found 2006.0.

### *d*(CGGTTGAU-NA) (7)

Yield: 85%, as determined based on the HPLC integration of the crude; HPLC gradient: 0% B for 10 min to 30% B in 30 min, $Rt = 29.4$ min; MALDI-TOF MS $m/z$ for $C_{90}H_{110}N_{32}O_{50}P_7$ $[M–H]^-$: calcd 2656.9, found 2655.7.

### UV-melting experiments

UV-melting experiments were performed as reported previously (29). The extinction coefficients of the hybrids were calculated as the sum of the extinction coefficients of the DNA portion and an $\varepsilon_{260}$ for nalidixic acid of 22 000 $M^{-1}$ $cm^{-1}$. $T_m$s are the extrema of the first derivatives of the 91-point smoothed curves, and hyperchromicities are $\Delta E_{260}$ between high and low temperature baselines, and divided by the $E_{260}$ at low temperature.

### Sample preparation and NMR spectroscopy

The modified DNA was lyophilized three times from 10% aqueous $NH_3$ and twice from $D_2O$. A sample of **6** (0.65 μmol) was taken up in phosphate-buffered saline buffer (200 μl; containing NaCl, KCl, $Na_2HPO_4$ and $KH_2PO_4$) made up in 99.9% $D_2O$ to pH 7 (uncorrected for deuterium effect) and transferred to a susceptibility-matched NMR tube (Shigemi Co., Tokyo, Japan). For spectra containing signals of exchangeable protons, the solution was dried and the residue taken up in $H_2O/D_2O$ (9:1, 230 μl). Spectra for generating constraints were acquired on a Bruker Avance 800 spectrometer at Bruker Biospin (Rheinstetten, Germany) at 283 K and spectral widths of 8741 ($D_2O$ samples) and 15 432 Hz ($H_2O/D_2O$, 9:1 samples). Suppression of the excess solvent peak was achieved by presaturation during the recycle delay ($D_2O$ samples) or the WATERGATE gradient pulse sequence (32) ($H_2O/D_2O$ samples). Relaxation times were assumed to be similar to those reported for other modified DNA hexamer duplexes (33). The repetition delay was set to 2 s, a value larger than the T1 times estimated from inversion-recovery experiments. Data acquired included NOESY spectra at mixing times of 62.5, 150 and 250 ms, DQF-COSY, TOCSY and HSQC spectra. Spectra were recorded with 256, 512 or 1024 increments in F1 and 8000 in F2, 16 or 32 scans per increment and were processed using XWINNMR (Bruker Instruments) and Sparky (version 3, available from Drs T. D. Goddard and D. G. Kneller, UCSF).

### Resonance assignments

The resonances of the methyl and ethyl groups of the nalidixic acid residue were identified in the 1D spectrum, and the assignments were confirmed in NOESY, COSY and TOCSY spectra. The aromatic protons of the nalidixic acid were identified based on NOESY crosspeaks to the methyl and ethyl groups. Sequential assignment of H1′ and H6/8 protons of the nucleotides of the pentamer *d*(CGCGU) followed an established protocol for duplex DNA (34–36). Starting from H1′ signals of each nucleotide, the spin systems of the deoxyriboses were assigned via TOCSY and COSY crosspeaks. The resonances of H2′ and H2″ were stereospecifically assigned based on the intensity of crosspeaks to H1′, H3′ and H5′/H5″ in the NOESY spectrum at 62.5 ms mixing time (H1′ is closer to H2″, H3′ and H5′ were assumed to be closer to H2′). Further, their COSY crosspeaks to H3′ were inspected. All H2′ resonances were found to be upfield of H2″, as expected for B-form DNA (37). The resonances H5′/H5″ were stereospecifically assigned, if possible, based on the scalar coupling to H4′ (38) and the assignment was confirmed based on the distances to neighboring protons in refined structures. The resonance of H2 of A1 was the only unassigned singlet left in the aromatic region, which also led to the deoxyribose spin system of A1 via the H2–H1′ crosspeak. Resonance H6 of U6 led to the ribose spin system via a NOESY crosspeak. The exchangeable protons were assigned starting from the resonances of H1 of the dG residues in the low-field region of the spectra acquired in $H_2O/D_2O$. The strongest NOESY crosspeak to H1 was assigned to H42 of the pairing dC residue, which led to H41. Strong crosspeaks from H41 to H5 of the respective dC residue provided the assignment to a specific base pair. The amidic NH at position 2′ of the dU residue was identified based on NOESY crosspeaks to neighboring H1′ and H2′ resonances. Of residue A1, only one resonance was found for the amino group at position 6, which was assigned by the crosspeak to A1H2 and by the peaks to the nalidixic acid moiety after the general structure of the duplex was known. The protons H21 and H22 of the dG residues and H3 of uridine were not observed, probably due to rapid exchange with solvent.

### Constraints

Crosspeaks in a NOESY spectrum of a $D_2O$ solution of **6** with a mixing time of 250 ms were integrated using Sparky, producing intensities that were used to calculate initial interproton distances via the isolated spin system approximation. Known distances, such as those between vicinal aromatic protons in cytosine, uracil and nalidixic acid or those between geminal protons of methylene groups, were used for calibration. Besides fixing a general value for spectral noise, each peak was assigned its own error percentage. The errors used were 10% for all well-resolved peaks, integrated by fitting a Gaussian peak shape, and 20% for peaks within 0.33 ppm of the diagonal. Some of the errors thus determined automatically were adjusted manually after judging the peak and its surrounding background. After the general structure of the complex had been established, based on over 60 unambiguous NOE-derived distance constraints, a significant contribution of interstrand NOEs between protons of the deoxyriboses of the core tetramer could be excluded. The initial structures were used to compute refined distance constraints in MARDIGRAS (39) from integration values of NOESY crosspeaks via relaxation matrix calculations. The RANDMARDI version of the software was used to account for integration error and spectral noise (40) (>10 model structures, 500 samples, in 4–50 iterative steps each). Calculations were run with 3.5 and 4.5 ns

correlation time, assuming isotropic tumbling, for NOESY spectra at three mixing times (62.5, 150 and 250 ms). The results from all six calculations were averaged using the 'avgmar' routine of MARDIGRAS. The values of 'low1' and 'up2' of the averaging step were used as upper and lower bounds of the constraints, yielding constraint boundaries ranging from ±0.2 to ±2 Å, with an average value of ±1 Å. Hydrogen bonding constraints were entered for the Watson–Crick base pairs of the $(CGCG)_2$ core, and between NH6 of A1 and O3′ of U6. Omitting the latter does not affect the fold of $(\mathbf{6})_2$. Further, very weak NCS constraints (weight = 3, *B*-value = 15) were used for the calculation of the final structures, to facilitate the generation of more symmetrical dimers. Constraints based on trivial crosspeaks, solely defining the primary structure, were not entered. The resonances of the H1′ protons of the residues of the core tetramer appear as triplets with the sum of the coupling constants >12 Hz. Further, H2′′–H3′ and H3′–H4′ crosspeak patterns in DQF-COSY spectra are consistent with B-form DNA. Therefore, a B-type dihedral angle constraint for backbone angle γ of C4 was entered with boundaries of ±30°. Restraining all backbone angles of the core tetramer with values typical for B-form DNA analogously to calculations reported for other DNA hexamers (29,41) did not alter the fold of $(\mathbf{6})_2$. During refinement, separate calculations were performed for the two stacking modes of dangling residue A1. For one set of these, six additional NOE-based constraints were entered for A1 in syn conformation. For calculations focused on A1 in anti conformation, two other NOE-based constraints and one repulsive constraint were entered. Omitting the repulsive constraint during restrained molecular dynamics (MD) gave occasional structures where A1 was in the minor groove, a location for this residue in clear violation of the existing NOE information, thus lowering the yield of accepted structures, but does not change the fold of $(\mathbf{6})_2$. The constraints used for either focused set of calculations are given in Supplementary Table S3. Omitting these constraints yields structures with the same fold as that seen in the focused calculations, except for a poorly defined localization of A1.

### Structure generation

Generation of topology files and coordinates for extended strands, as well as restrained MD calculations themselves, were carried out in CNS (42), version 1.1, on LINUX platforms, compiled with Intel ifc compiler, version 6.0. For the unmodified part of the DNA, parameters supplied with CNS were used. For the 2′-amino modified uridine, the CNS parameters for uridine were used, with a patch exchanging the 2′ oxygen to an NH group. Structural parameters for the nalidixic acid residue were calculated at the level HF/4-21G** in Gaussian 94, converted to CNS format with Xplo2D 3.2.1 (43), and carefully edited to remove unnecessary improper, dihedral and angle constraints. Restrained MD calculations were performed in CNS, using the torsion angle MD option (44) with setting identical to those employed in earlier work (41). See Table 5 in Ref. (45) for a compilation of the computational steps. The methyl group M9 and the ethyl group of the cap were excluded from this NCS potential. For refinement, restraint violations and restraint distribution over the structure were visualized using VMD (46) and a plug-in for visualizing the entered constraints and error bounds written in-house. Back-calculated NOESY spectra were generated with CORMA from the MARDIGRAS package, using the full relaxation matrix, and displayed in Sparky. Table 1 comprises data on constraints used, and Supplementary Figures S1 and S12 show constraints defining the position of N7 and the central G3C4 dinucleotide in graphical form.

**Table 1.** Constraints[a] used for MD calculations on $(\mathbf{6})_2$ and results

| | Conformation I[b] | Conformation II[b] |
|---|---|---|
| NOE-based constraints (total) | 252 | 246 |
| Interresidue | 172 | 170 |
| Intraresidue | 80 | 76 |
| Dihedral angle constraints | 2[c] | 2[c] |
| Hydrogen bonding constraints | 12/14[d] | 12/14[d] |
| Base pair planarity constraints | 8 | 8 |
| Violations: no violations of distance and dihedral constraints | | |
| Statistics for the 10 lowest energy structures | | |
| r.m.s.d. (Å) from average (all atoms) | 0.60 | 0.71 |
| (backbone) | 0.71 | 0.75 |

[a]Given is the total number of constraints entered for calculations involving both strands of the symmetrical dimer.
[b]Constraints for conformations I (A1 adopts syn conformation) and II (A1 adopts anti conformation) differ only in constraints to and within A1. See Supplementary Table S3 for a listing.
[c]Only the dihedral angle γ of C4 was constrained.
[d]For the core tetramer, 12 H-bond constraints for base pairs were used, loose H-bond constraints between NH6 of A1 and O3′ of U6 were entered but proved inconsequential for the structures obtained.

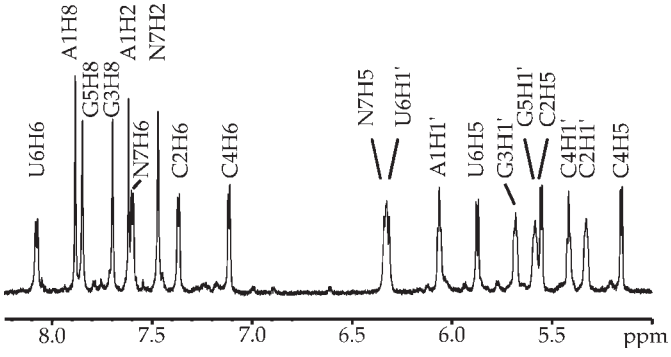


**Figure 3.** Low field region of the $^1$H-NMR spectrum of *d*(ACGCGU-NA)$_2$ $(\mathbf{6})_2$ in buffered $D_2O$ at 800 MHz and 283 K.

## RESULTS

The 1D NMR spectrum of duplex $(\mathbf{6})_2$ shows one predominant set of signals and some truly minor signals (⩽5% intensity) that are too small to allow for assignment (Figure 3). Although the material used was purified by HPLC and MALDI-TOF MS (see Supplementary Material), we cannot rigorously exclude that these signals are caused by residual failures from the synthesis. It is also possible that $(\mathbf{6})_2$ can adopt an additional state of much lower stability, in which the quinolone is not intercalated. Given the very low intensity of these additional signals, no attempts were made to pursue them further. For the dominating set of signals, sequential assignment of the H1′ and H6/8 resonances (34–36) was possible for the core tetramer

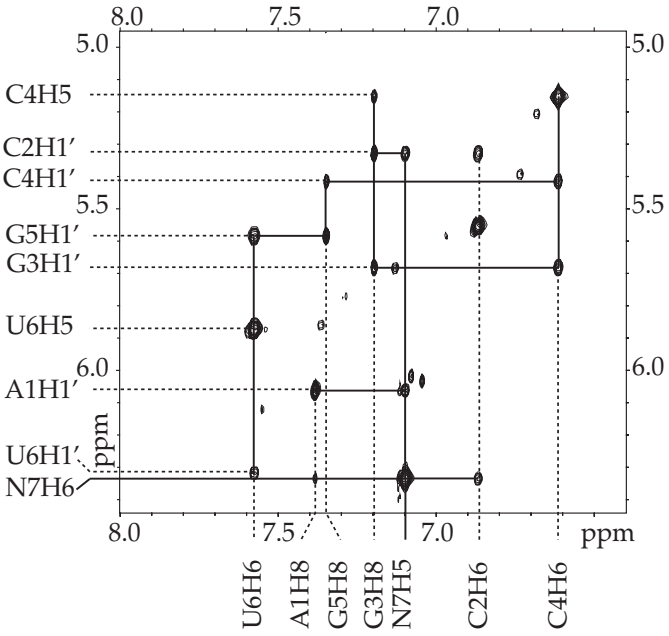


**Figure 4.** Expansion of the NOESY spectrum of $(\mathbf{6})_2$ in buffered $D_2O$ at 800 MHz, 283 K and 250 ms mixing time showing NOE connectivities between H1′ resonances of the ribose systems, protons of the nucleobases and resonances of the nalidixic acid residue.

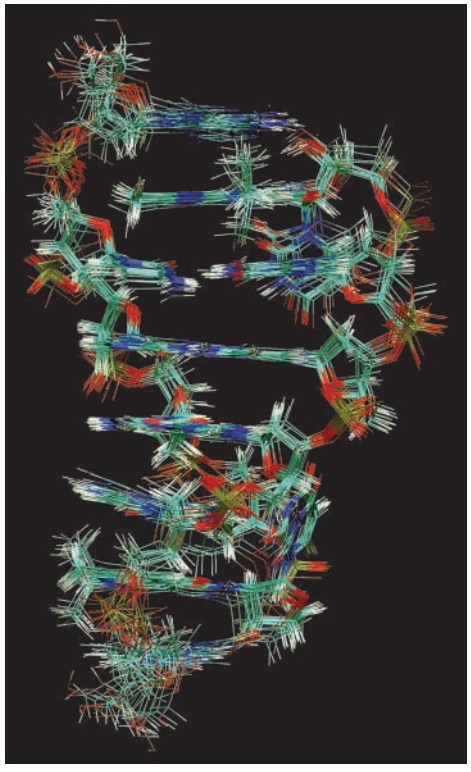

**Figure 5.** Overlay of 20 lowest energy structures of $(\mathbf{6})_2$, as obtained by restrained torsion angle MD. Ten structures each were obtained from calculations with constraints favoring stacking of A1 in syn and anti conformation. The graphic was generated with VMD (46). See Supplementary Figure S13 for separate overlays of structures from either conformation.

*d*$(CGCG)_2$, and the nalidixic acid residue gave NOEs to both C2 and U6 (Figure 4), suggesting that the terminal portion of the duplex featured an intercalated quinolone. In the spectrum acquired from a solution of $H_2O/D_2O$, peaks for the imino protons of the C:G base pairs were observed in the typical chemical shift range >12 ppm A comparison with the unmodified control duplex $(ACGCGU)_2$ shows significant chemical shift differences of >0.2 ppm for either H1′ and/or nucleobase resonances of residues A1, C2, G5 and U6 (Supplementary Figures S9 and S10). Restrained torsion angle MD (44) with distance constraints based on integration of NOESY crosspeaks gave a first set of structures with the quinolone rings displacing the terminal U:A base pairs. The structure was subjected to refinement based on a relaxation matrix treatment of the NOESY crosspeak intensities. Overall, >300 MD calculations, each leading to at least 80 individual structures, were performed to refine the structure.

Conflicting constraints involving residue A1 initially complicated the refinement. For example, H2 of this residue's nucleobase shows NOEs to neighboring protons located in the major groove and to neighboring protons pointing toward the minor groove. This suggests that the dangling residue is not fixed and adopts more than one conformation on the NMR time scale. This is consistent with the sligthly reduced line widths observed for H2 and H8 of A1, which indicate increased mobility. The half height peak widths for these resonances at 10°C are 4.7 and 4.9 Hz, whereas those of H8 of G3 and G5 are 5.3 and 5.8 Hz. A set of $^1$H-NMR spectra acquired at 5°C temperature intervals shows that resonances of A1, such as H1′, broaden only moderately when the duplex begins to melt at 45°C, and re-sharpen at 60°C, a temperature where resonances of the core duplex are still broad. This confirms that the 3′-terminal residue does engage in detectable interactions with the duplex but becomes fully disordered at a lower temperature than the nucleotides forming Watson–Crick base pairs.

Rather than letting this residue rotate freely in calculations, attempts were made to identify states in which A1 comes within stacking distance to the neighboring residues, resulting in the NOESY crosspeaks observed. Two conformations that show stacking of A1, albeit in different arrangements relative to the remainder of the structure, and with either a syn or an anti conformation for A1 itself, were thus generated. Together, they fully explain the NOEs observed in the NOESY spectra. The crosspeak between H8 and H1′ of A1 is between 4.5 and 6 times more intense than those of the other purines in the NOESY spectra acquired, as expected for a residue adopting a syn conformation. An overlay of a total of 20 lowest energy structures, 10 each from either conformation, is shown in Figure 5. Figure 6 shows an overlay of the experimental and the back-calculated NOESY spectrum of $(\mathbf{6})_2$, and Table 1 provides detailed information on the structures. It is important to emphasize that the remainder of the complex is unaffected by the dangling motions of A1. This can be seen from Figure 5 and Supplementary Figure S11 where an overlay of the back-calculated NOESY spectra from either conformation is shown.

In either of the two stacked conformations, A1 places about half of the surface of its purine ring system on the quinolone moiety (Figure 7). The adenine ring is also close enough to the ribose ring of U6 to allow for at least transient hydrogen

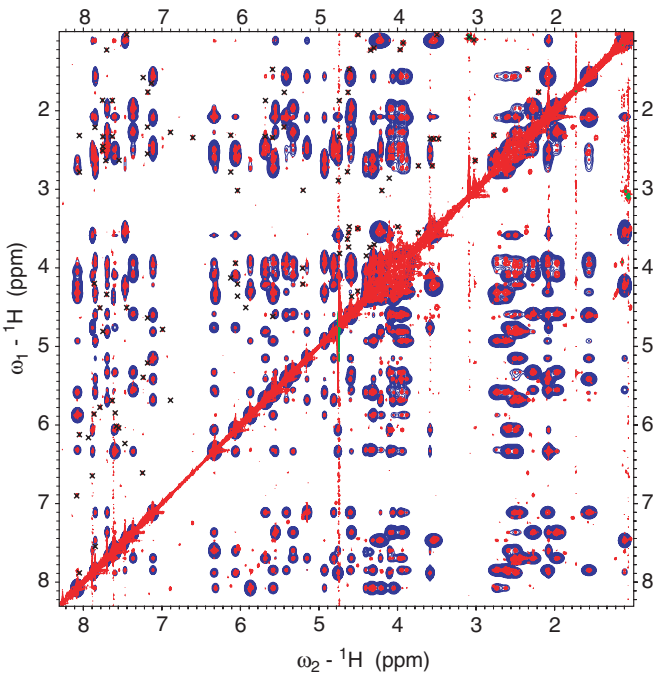


**Figure 6.** Overlay of experimental (red) and back-calculated (blue) NOESY spectrum of $(\mathbf{6})_2$ (conformation II). The experimental spectrum was acquired in phosphate-buffered $D_2O$ at 250 ms mixing time, 283K (red), and the back-calculated one was generated from the averaged structure of the 10 lowest energy conformations in CORMA at 250 ms mixing time and 3.5 ns correlation time, imported into Sparky. Crosspeaks originating from the unidentified minor resonances (cf. Figure 3) are labeled with crosses. Line widths in the back-calculated spectrum were increased to facilitate visual inspection. For a comparison of the back-calculated spectra of the two conformations that differ in the stacking mode of A1, see Supplementary Figure S11.

bonding with the 3′-hydroxyl group of this nucleotide. In the spectra of $(\mathbf{6})_2$ in $H_2O/D_2O$, a signal is observed above 6 ppm that was assigned to NH6 of A1. In the syn-like conformation I of this nucleoside several structures show a H-bonding distance to O3′ of U6. This putative hydrogen bonding interaction, in which NH6 of A1 acts as donor and O2 of U6 as acceptor is highlighted in Figure 8. In stacking mode II, where A1 adopts the anti conformation, a similar hydrogen bond is possible. Figure 8 also shows an additional possible hydrogen bond between O2 of U6 and NH2 of G5 that can be inferred from the spatial closeness of donor and acceptor groups, but could not be detected directly in this solvent-exposed position. In either stacking mode of A1, the pyrimidine is close enough to the purine's amino group to allow for this interaction.

The terminal residues can arrange themselves into a tightly packed structure in either conformation. The kink in the backbone between G5 and U6 places the ribose ring of U6 vertically above the deoxyribose of G5. The ribose ring thus complements the quinolone in taking up the space usually occupied by a base pair. The methyl group at position 7 of the nalidixic acid residue stacks against the deoxyriboses and A1 and C2, and the ethyl group at position 1 is located in the major groove, where it can engage in (transient) hydrophobic interactions with the neighboring nucleotides. The orientation of this ethyl group is not well fixed in space, though, as evidenced by NOEs to protons from several surrounding residues.

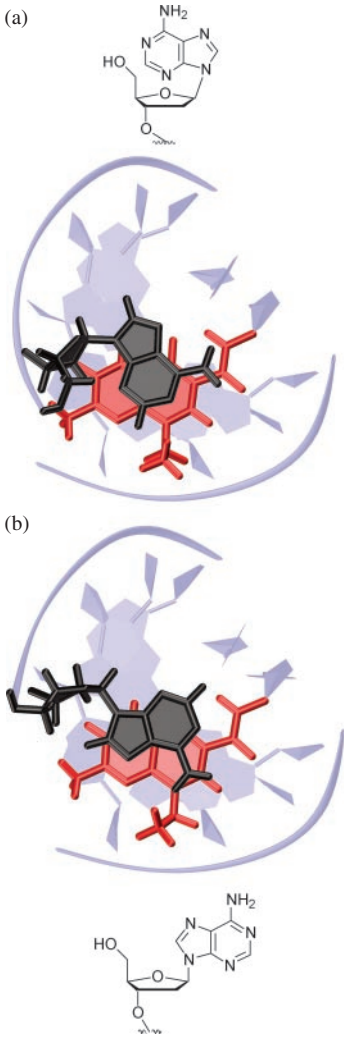


**Figure 7.** Two stacking modes of A1, representing the extremes of the accessible conformational states for the dangling residue. Each portion of the figure shows two different representations, one a structural drawing of A1, and one a view from the top along the axis of the helix. (**a**) Conformation I in which A1 adopts a syn-arrangement, (**b**) conformation II in which A1 adopts an anti-arrangement. Each stacking arrangement was calculated using a different subset of NOE constraints for A1 and N7 (Supplementary Table S3).

The global shape of the disrupted duplex is surprisingly similar to that of an undisturbed Watson–Crick double helix, and the displaced nucleotides do not lead to a 'bubble' in the helix. The core duplex $d(CGCG)_2$ also shows a largely undisturbed Watson–Crick geometry.

We next studied whether the base pair-disrupting mode of binding of the nalidixic acid residue is also found in the presence of a weak neighboring base pair. The non-self complementary octamer **7** (Figure 9) was synthesized (27), where the quinolone-bearing 3′-terminal deoxyuridine residue is next to a dA residue. When subjected to UV-monitored melting analysis in the presence of the fully matched target strand, **7** gave a 5.5°C higher $T_m$ than that of the unmodified control duplex (Table 2). Duplexes with a mismatched nucleobase at the 5′-terminal position of the target did not lead to a significant decrease in the $T_m$, suggesting that U8 does not form a base pair. At the penultimate position, however, there is good

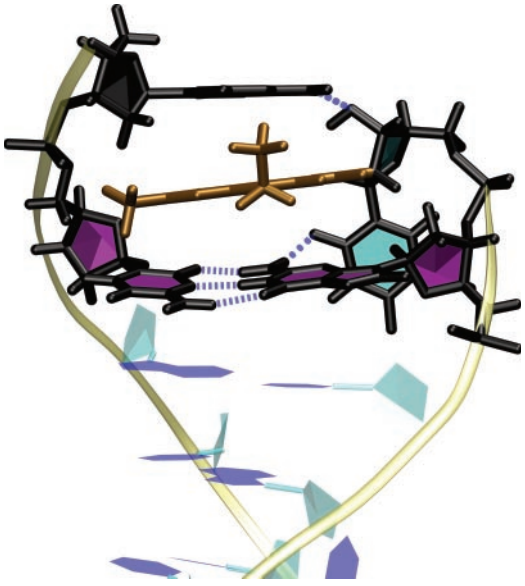

**Figure 8.** Terminus of $(\mathbf{6})_2$ with A1 in anti conformation, viewed from the major groove. Putative hydrogen bonds are shown as blue dotted lines and the hydrogen bonds in the Watson–Crick base pair as broken blue lines. The quinolone is shown in gold, the ring systems of A1 and U6 are filled in turquoise, and those of the C2:G5 base pair are filled in purple. The backbones of the DNA are traced as yellow ribbons, and the nucleotides of the remainder of the duplex are shown in cartoon style.

base pairing fidelity, with $T_m$ decreases of up to 11.4°C when mismatches are placed in the target strand. These observations are in agreement with the notion that the nalidixic acid residue forces a similar structure onto the terminal region of the duplex of **7** with its target strand as it does in $(\mathbf{6})_2$.

Finally, results from exploratory work with compound **8** (Figure 9), which was prepared in the context of a combinatorial study, suggests the base pair-disrupting binding mode of a quinolone (in this case cinoxacin) is also induced when the nucleobase of the quinolone-bearing residue is adenine rather than uracil. When $(\mathbf{8})_2$ was subjected to degradation with bovine spleen nuclease, which digests oligonucleotides from the 5′-terminus, its terminal thymidine residue was readily cleaved off, whereas the penultimate nucleotide was removed more slowly under nuclease attack than that of the unmodified control $d(\mathrm{TGCGCA})_2$. This suggests that the terminal residue is sterically accessible, but the penultimate one is shielded from nuclease attack (Supplementary Figure S7). This implies that the quinolone again disrupts the terminal base pair and stacks on the penultimate C:G base pair.

## DISCUSSION

Quinolones such as nalidixic acid are too small to act as classical intercalators. The current structures show one possible mode of binding to DNA that is open to these drug molecules, at least when they are covalently attached to a nucleotide of a weak U/T:A base 'pair'. The quinolone-containing terminal region has a global shape reasonably similar to that of the remainder of the DNA helix and is well packed. The drug places itself below one unpaired nucleotide (A1) and engages the ribose ring of another (U6) in filling

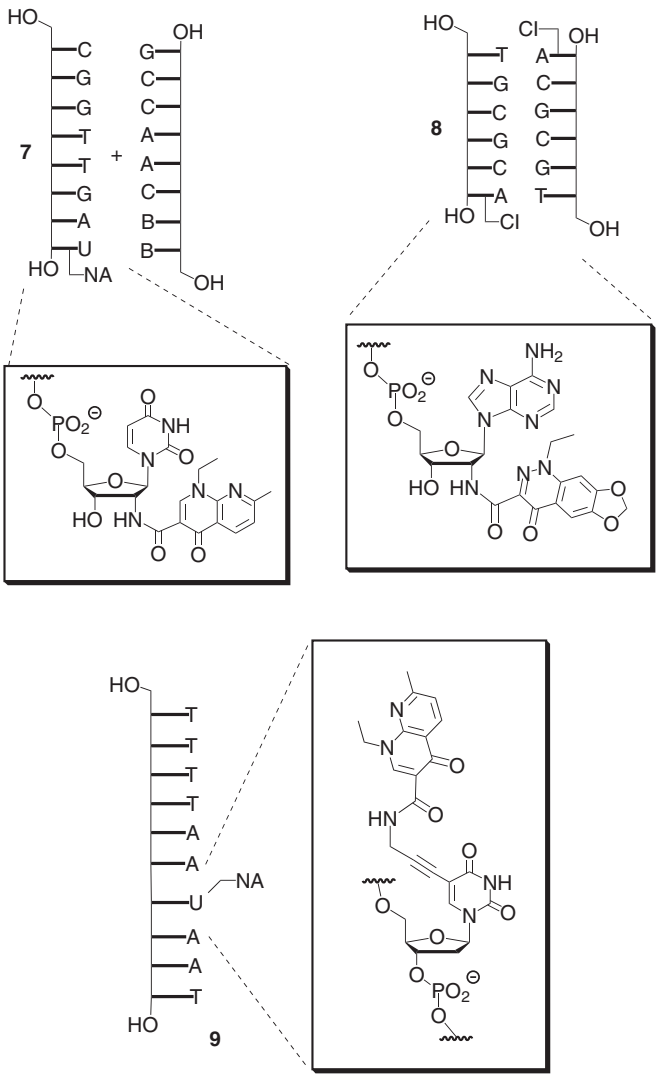





**Figure 9.** Structures of quinolone-DNA hybrids.

some of the space vacated by the missing base pair. The bicyclic quinolone alone is only slightly bigger than a single purine residue, and would be unable to fill the space of a base pair by itself. The 'hemi-intercalation' places the nucleobase of U6 in the minor groove of the DNA helix, a site well known for attracting small molecules. In the structure of $(\mathbf{6})_2$, the extent to which the ribose ring of the quinolone-bearing residue is pulled over the plane of the last intact base pair is greater than in the structure of the oxolinic acid-bearing hexamer $d(\mathrm{OA\text{-}TGCGCA})_2$ (29), but the phenomenon is also observed in the earlier structure. Unlike the 5′-linked oxolinic acid, the 3′-linked nalidixic acid does not force the nucleobase of the target strand into the minor groove, but that of the nucleotide to which it is attached.

Duplex-destabilizing effects of quinolone residues appended to residues in the interior of oligonucleotides have also been observed. The DNA decamer **9** (Figure 9) was recently prepared via solid-phase synthesis and studied in UV-melting experiments (47). This nalidixic acid-bearing oligonucleotide gives a $T_m$ with its fully complementary DNA target strand below 15°C, even at 1 M salt, consistent with the assumption

**Table 2.** UV-melting data for octamer **7** or control strand CGGTTGAT with target strands

| Probe[a] | Target sequence | Mismatch | $T_m$ (°C)[b] [salt] = 150 mM | [salt] = 1 M | $\Delta T_m$ to perfect match at 1 M salt (°C)[c] |
|---|---|---|---|---|---|
| CGGTTGAT | **A**TCAACCG | | 30.1 ± 0.5[d] | 34.3 ± 0.6[d] | |
| CGGTTGAU-NA | **A**TCAACCG | | 34.4 ± 0.7[d] | 39.8 ± 0.7[d] | |
| CGGTTGAT | **C**TCAACCG | T:C | 23.7 ± 0.8 | 28.4 ± 0.9 | −5.9 |
| CGGTTGAU-NA | **C**TCAACCG | U:C | 33.6 ± 0.9 | 39.2 ± 0.7 | −0.6 |
| CGGTTGAT | **G**TCAACCG | T:G | 25.8 ± 0.6 | 30.2 ± 0.8 | −4.1 |
| CGGTTGAU-NA | **G**TCAACCG | U:G | 34.2 ± 1.0 | 39.8 ± 0.7 | 0 |
| CGGTTGAT | **T**TCAACCG | T:T | 24.4 ± 0.7 | 29.4 ± 1.0 | −4.9 |
| CGGTTGAU-NA | **T**TCAACCG | U:T | 33.4 ± 0.8 | 39.4 ± 0.7 | −0.4 |
| CGGTTGAT | A**A**CAACCG | A:A | 21.4 ± 0.2 | 26.7 ± 0.7 | −7.6 |
| CGGTTGAU-NA | A**A**CAACCG | A:A | 28.2 ± 1.3 | 32.8 ± 0.7 | −7.0 |
| CGGTTGAT | A**C**CAACCG | A:C | 20.3 ± 0.7 | 25.1 ± 0.9 | −9.2 |
| CGGTTGAU-NA | A**C**CAACCG | A:C | 23.0 ± 1.0 | 28.5 ± 1.1 | −11.3 |
| CGGTTGAT | A**G**CAACCG | A:G | 23.7 ± 0.7 | 28.1 ± 0.7 | −6.2 |
| CGGTTGAU-NA | A**G**CAACCG | A:G | 27.3 ± 1.0 | 32.2 ± 0.7 | −7.6 |

[a]Sequences are given 5′- to 3′-terminus; U denotes 2′-amino-2′-deoxyuridine residue and NA the residue of nalidixic acid. Nucleobases at positions where mismatches were introduced are given in boldface.
[b]Average of four $T_m$s ± SD at 1.5 μM strand concentration and $NH_4OAc$ concentration given as [salt].
[c]$T_m$ difference to duplex with fully complementary target at 1 M $NH_4OAc$.
[d]These values were determined independently from those in reference (27), and agree with the literature values within the error margins.

that the quinolone interferes with base pairing at a central point of the duplex. This is surprising as the nalidixic acid is linked to position 5 of a dU residue via an alkynyl linker that should place it in the major groove without causing any steric conflicts.

The base pair-disrupting binding mode of the nalidixic acid residue in $(\mathbf{6})_2$ is not a necessary consequence of its site or mode of covalent attachment. The residue of anthraquinone carboxylic acid, e.g. a structurally similar aromatic acid, when linked to the amino group of a 3′-terminal 2′-amino-2′-deoxyuridine residue of AGGTTGAU, leads to improved base pairing fidelity at the terminus (23), including good base pairing fidelity of U8 itself. This suggests that the residue of this aromatic acid does not disrupt the terminal base pair. The same is true for some aromatic substituents, such as pyrene butyric acid, attached to the position 5 of deoxyuridine residues in the interior of DNA strands via an alkynyl spacer. These stabilize DNA duplexes (47) and do not abolish base pairing selectivity. The same is true for certain other carboxylic acid residues 5′-linked to oligonucleotides (22,48).

To those who wish to develop molecular caps that seal the termini of duplexes between hybridization probes and target strands (22,48,49), the structure of $(\mathbf{6})_2$ may seem disappointing. The quinolone not only fails to cap the terminal base pair, it favors its disruption. But, the entire acylated nucleotide (U6-N7) may be treated as one large 'composite cap' that can seal off a terminus. In the structure of $(\mathbf{6})_2$, the residues U6 and N7 together cap the base pair G5:C2. They thus provide a blueprint for a simplified cap of the same shape. A simplified and easy-to-synthesize cap has been described recently for 5′-termini that contains a pyrrolidinol moiety instead of a ribose residue and a pyrenylmethyl group as stacking unit (23). Even though this simplified cap can be synthesized in two steps from commercially available starting materials, it markedly increases duplex stability, it improves base pairing fidelity and it protects against exonuclease attack. To develop a similar solution in the current case, e.g. in the form of an aminodeoxyribose nalidixate, is attractive, as known 3′-caps are less satisfactory in terms of their fidelity-increasing effect than their best 5′-attached counterparts (23,48,49). Other applications of 2′-linked quinolone–DNA hybrids may emerge in the field of DNA-based nanostructures (50). If one was to employ the residue of a different quinolone than nalidixic acid, which carries a substituent at position 7 of the quinolone scaffold that can act as a starting point for DNA synthesis, the resulting 'branching' strand can be expected to protrude from a helix at an angle of ∼90°, if the quinolone positions itself like N7 in the structure of $(\mathbf{6})_2$. A T-like structure is a motive that has achieved a certain prominence in the field of DNA-based nanostructuring, as evidenced by the dsDNA segments joined by Holliday junctions (51).

Perhaps the most interesting is the possible relevance of the structure of $(\mathbf{6})_2$ for the biological activity of quinolones. We are tempted to speculate that the structure observed could be similar to that formed with DNA in the active site of gyrases. There are certain arguments that make this reasonable. Firstly, it seems as if the position of N7 in $(\mathbf{6})_2$ could also be adopted by other quinolones, including highly active gyrase inhibitors. All clinically important quinolones possess substituents at positions 1 and 7 of the heterocyclic ring system. Positions 1 and 7 are not tightly encased in the structure of $(\mathbf{6})_2$ and bulkier substituents might be accommodated there. Both the cyclopropyl group at position 1 of drugs such as ciprofloxacin and the piperazine moiety found at position 7 of this and related drugs (e.g. norfloxacin or pipemidic acid) should find sufficient space in the major groove of helices with a structure similar to that of $(\mathbf{6})_2$. Secondly, the structure of $(\mathbf{6})_2$ also leaves space for purines instead of pyrimidines at the position currently occupied by U6. The minor groove is open below the uracil of U6 and should accommodate these larger nucleobases, as corroborated by the nuclease survival results for **8** (*vide supra*). Therefore, other sequence motives than the one studied here should be able to adopt the quinolone-induced fold.

Thirdly, the interactions between the quinolone and the DNA are very strong. At 1 M salt, the UV-melting temperatures for $(\mathbf{6})_2$ and control $d(ACGCGT)_2$ are 53.1 and 31.1°C,

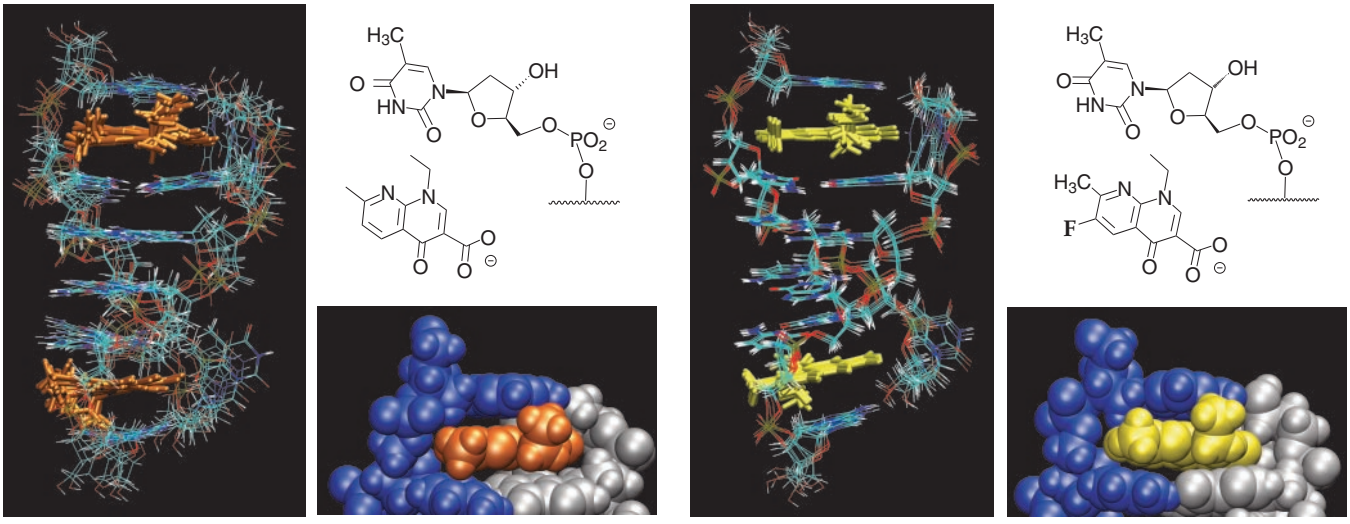


**Figure 10.** Modelled structures of non-covalently linked quinolone–DNA complexes generated via molecular dynamics using restrains obtained for $(\mathbf{6})_2$. Left: nalidixic acid (orange) as ligand for $(ACGCGT)_2$; Right: 6-fluoronalidixic acid (yellow) as ligand for $(ACGCGT)_2$. For each structure, an overlay of low energy structures (larger images), a two dimensional representation of the primary structures, and a space filling model of the terminal region are shown. Coordinates of the complexes are given in the Supplementary Tables S4 and S5.

respectively (27). The 11°C $T_m$ increase per modification is more than that an additional base pair would provide, even if it was a C:G base pair. Since $(\mathbf{6})_2$ shows only 4 bp, one might also compare the 53.1°C with the $T_m$ of the core tetramer duplex $d(CGCG)_2$. For the latter, HyTher (52) predicts a $T_m$ of 2.2°C at 4 μM total strand concentration and 1 M monovalent salt, i.e. 50°C below that of the nalidixic acid-containing duplex with its re-folded base pair, including a putative single H-bond between A1 and U6. It is not particularly probable that a small molecule like nalidixic acid has many different binding modes available that involve extensive favorable interactions. If it does bind to DNA in the active site of gyrases (and no model assumes that it does not) and manages to stall the gyrase, it will probably do so through strong favorable interactions. Finally, the shape of $(\mathbf{6})_2$ is globally not too different from that of a standard DNA helix. Nature evolved gyrases to act on dsDNA, and the active site must have evolved to fit that substrate. Given the size of dsDNA as a substrate, it is unlikely that a complex with a radically different shape would fit into the active site.

One interesting question is how much the covalent link affects the exact position of the quinolone relative to the DNA. This question is difficult to answer, as the covalent link seems to be necessary to prevent the 'blurring' of complexes that prevented the generation of high resolution structures in earlier NMR-studies on non-conjugated quinolone–DNA complexes (53). But, the covalent link also has an other noteworthy effect. It prevents the free association of quinolones into stacks of more than one drug molecule. The formation of stacks of four quinolones has been proposed in models of the biological mode of action of quinolones (54). What our structures and the $T_m$s of the duplexes show is that there is no need for the formation of quinolone–quinolone complexes for very strong interactions with DNA to occur.

To demonstrate that the current high resolution structure may be a useful starting point for modeling possible ternary complexes of gyrases, quinolones and DNA, we generated two non-covalent quinolone–DNA complexes based on the structure of $(\mathbf{6})_2$ (Figure 10). The coordinates for these complexes are given in the Supplementary Material. The first is a non-covalent complex of nalidixic acid with the DNA duplex $(ACGCGT)_2$, the other is a complex between the same DNA and nalidixic acid with a fluoro-substituent at position 6, i.e. the position where second generation chinolone antibiotics are most frequently fluorinated. Either structure was generated by restrained MD in CNS (42), starting from the unmodified DNA hexamer and the respective quinolone as separate molecules. During the MD, which were performed exactly as in the case of $(\mathbf{6})_2$, the NMR-based constraints used for generating the structure of $(\mathbf{6})_2$ were applied, except for those constraints involving atoms not found in the non-covalently linked complex. The force field applied during these calculations ensures physically reasonable structures. Inspection of Figure 10 shows that the structures obtained are tightly folded with good shape complementarity between DNA and quinolones. In either case, the interactions are favorable, with total energies calculated by CNS below −400 kcal/mol. The non-covalent structures show features of the qualitative model for quinolone–DNA complex in the active site of gyrases proposed by Maxwell and co-workers (30,31) and should provide a possible starting point for modeling ternary complexes with the enzyme.

## SUPPLEMENTARY MATERIAL

Supplementary Material is available at NAR Online.

## ACKNOWLEDGEMENTS

The authors wish to thank Dr Rainer Kerssebaum (Bruker Biospin) for the acquisition of NMR spectra at 800 MHz,

A. Friemel, P. Lang and Dr A. Rapp for help with experiments at lower field strength, and J. Tuma for helpful discussions. This work was supported by DFG (grant RI 1063/1). Funding to pay the Open Access publication charges for this article was provided by The University of Karlsruhe.

*Conflict of interest statement*. None declared.

## REFERENCES

1. Hardman,J.G., Limbird,L.E., Molinoff,P.B., Ruddon,R.W. and Goodman,G.A. (eds) (1996) 44. Antimicrobial Agents. In *The Pharmacological Basis of Therapeutic, 9th edn*. McGraw-Hill, NY, pp. 1065–1068.
2. Jacobs,M.R. (2004) Fluoroquinolones as chemotherapeutics against mycobacterial infections. *Curr. Pharm. Des.*, **10**, 3213–3220.
3. Drlica,K. and Zhao,X. (1997) DNA gyrase, topoisomerase IV, and the 4-quinolones. *Microbiol. Mol. Biol. Rev.*, **61**, 377–392.
4. Roca,J. and Wang,J.C. (1992) The capture of a DNA double helix by an ATP-dependent protein clamp: a key step in DNA transport by type II DNA topoisomerases. *Cell*, **71**, 833–840.
5. Sugino,A., Peebles,C.L., Kruezer,K.N. and Cozzarelli,N.R. (1977) Mechanism of action of nalidixic acid: purification of *Escherichia coli* nalA gene product and its relationship to DNA gyrase and a novel nicking-closing enzyme. *Proc. Natl Acad. Sci. USA*, **74**, 4767–4771.
6. Chen,C-R., Malik,M., Snyder,M. and Krlica,K. (1996) DNA gyrase and topoisomerase IV on the bacterial chromosome: quinolone-induced DNA cleavage. *J. Mol. Biol.*, **258**, 627–637.
7. Wigley,D.B., Davies,G.J., Dodson,E.J., Maxwell,A. and Dodson,G. (1991) Crystal structure of an N-terminal fragment of the DNA gyrase B protein. *Nature*, **351**, 624–629.
8. Morais Cabral,J.H., Jackson,A.P., Smith,C.V., Shikotra,N., Maxwell,A. and Liddington,R.C. (1997) Crystal structure of the breakage–reunion domain of DNA gyrase. *Nature*, **388**, 903–906.
9. Tsai,F.T., Singh,O.M., Skarzynski,T., Wonacott,A.J., Weston,S., Tucker,A., Pauptit,R.A., Breeze,A.L., Poyser,J.P., O'Brien,R. *et al.* (1997) The high-resolution crystal structure of a 24-kDa gyrase B fragment from *E.coli* complexed with one of the most potent coumarin inhibitors, clorobiocin. *Proteins*, **28**, 41–52.
10. Dao-Thi,M.H., Van Melderen,L., De Genst,E., Buts,L., Ranquin,A., Wyns,L. and Loris,R. (2004) Crystallization of CcdB in complex with a GyrA fragment. *Acta Crystallogr D Biol. Crystallogr.*, **60**, 1132–1134.
11. Costenaro,L., Grossmann,J.G., Ebel,C. and Maxwell,A. (2005) Small-angle X-ray scattering reveals the solution structure of the full-length DNA gyrase a subunit. *Structure*, **13**, 287–296.
12. Noble,C.G. and Maxwell,A. (2002) The role of GyrB in the DNA cleavage-religation reaction of DNA gyrase: a proposed two metal-ion mechanism. *J. Mol. Biol.*, **318**, 361–371.
13. Corbett,K.D., Shultzaberger,R.K. and Berger,J.M. (2004) The C-terminal domain of DNA gyrase A adopts a DNA-bending beta-pinwheel fold. *Proc. Natl Acad. Sci. USA*, **101**, 7293–7298.
14. Shen,L.L. and Pernet,A.G. (1985) Mechanism of inhibition of DNA gyrase by analogues of nalidixic acid: the target of the drugs is DNA. *Proc. Natl Acad. Sci. USA*, **82**, 307–311.
15. Shen,L.L., Baranowski,J. and Pernet,A.G. (1989) Mechanism of inhibition of DNA gyrase by quinolone antibacterials: specificity and cooperativity of drug binding to DNA. *Biochemistry*, **28**, 3879–3885.
16. Noble,C.G., Barnard,F.M. and Maxwell,A. (2003) Quinolone–DNA interaction: sequence-dependent binding to single-stranded DNA reflects the interaction within the gyrase–DNA complex. *Antimicrob. Agents Chemother.*, **47**, 854–863.
17. Son,G.S., Yeo,J.-A., Kim,M.-S., Kim,S.K., Holmen,A., Akerman,B. and Norden,B. (1998) Binding mode of norfloxacin to calf thymus DNA. *J. Am. Chem. Soc.*, **120**, 6451–6457.
18. Shen,L.L., Mitscher,L.A., Sharma,P.D., O'Donnell,T.J., Chu,D.T.W., Cooper,C.S., Rosen,T. and Pernet,A.G. (1989) Mechanism of inhibition of DNA gyrase by quinolone antibacterials: a cooperative drug-DNA binding model. *Biochemistry*, **28**, 3886–3894.
19. Heddle,J. and Maxwell,A. (2002) Quinolone-binding pocket of DNA gyrase: role of GyrB. *Antimicrob. Agents Chemother.*, **46**, 1805–1815.
20. Llorente,B., Leclerc,F. and Cedergren,R. (1996) Using SAR and QSAR analysis to model the activity and structure of the quinolone–DNA complex. *Bioorg. Med. Chem.*, **4**, 61–71.
21. Altman,R.K., Schwope,I., Sarracino,D.A., Tetzlaff,C.N., Bleczinski,C.F. and Richert,C. (1999) Selection of modified oligonucleotides with increased target affinity via MALDI-monitored nuclease survival assays. *J. Comb. Chem.*, **1**, 493–508.
22. Mokhir,A.A., Tetzlaff,C.N., Herzberger,S., Mosbacher,A. and Richert,C. (2001) Monitored selection of DNA-hybrids forming duplexes with capped terminal C:G base pairs. *J. Comb. Chem.*, **3**, 374–386.
23. Narayanan,S., Gall,J. and Richert,C. (2004) Clamping down on weak terminal base pairs: oligonucleotides with molecular caps as fidelity-enhancing elements at the 5′- and 3′-terminal residues. *Nucleic Acids Res.*, **32**, 2901–2911.
24. Bugaut,A., Toulme,J.-J. and Rayner,B. (2004) Use of dynamic combinatorial chemistry for the identification of covalently appended residues that stabilize oligonucleotide complexes. *Angew. Chem. Int. Ed. Engl.*, **116**, 3206–3209.
25. Bugaut,A., Bathany,K., Schmitter,J.-M. and Rayner,B. (2005) Target-induced selection of ligands from a dynamic combinatorial library of mono- and bi-conjugated oligonucleotides. *Tetrahedron Lett.*, **4**, 687–690.
26. Sarracino,D.A. and Richert,C. (2001) Synthesis and nuclease stability of trilysyl dendrimer-oligodeoxyribonucleotide hybrids. *Bioorg. Med. Chem. Lett.*, **11**, 1733–1736.
27. Kryatova,O.P., Connors,W.H., Bleczinski,C.F., Mokhir,A.A. and Richert,C. (2001) A 2′-acylamido cap that increases the stability of oligonucleotide duplexes. *Org. Lett.*, **3**, 987–990.
28. Fan,J.-Y., Sun,D., Yu,H., Kerwin,S.M. and Hurley,L.H. (1995) Self-assembly of a quinobenzoxazin-Mg2+ complex on DNA: a new paradigm for the structure of a drug–DNA complex and implications for the structure of the quinolone bacterial gyrase–DNA complex. *J. Med. Chem.*, **38**, 408–424.
29. Tuma,J., Connors,W.H., Stitelman,D.H. and Richert,C. (2002) On the effect of covalently appended quinolones on termini of DNA-duplexes. *J. Am. Chem. Soc.*, **124**, 4236–4246.
30. Heddle,J.G., Barnard,F.M., Wentzell,L.M. and Maxwell,A. (2000) The interaction of drugs with DNA gyrase: a model for the molecular basis of quinolone action. *Nucleosides Nucleotides Nucleic Acids*, **19**, 1249–1264.
31. Mitscher,L.A. (2005) Bacterial topoisomerase inhibitors: quinolone and pyridone antibacterial agents. *Chem. Rev.*, **105**, 559–592.
32. Piotto,M., Saudek,V. and Sklenar,V. (1992) Gradient-tailored excitation for single-quantum NMR spectroscopy of aqueous solutions. *J. Biomol. NMR*, **2**, 661–665.
33. Gomez-Pinto,I., Marchan,V., Gago,F., Grandas,A. and Gonzalez,C. (2003) Solution structure and stability of tryptophan-containing nucleopeptide duplexes. *Chembiochem*, **4**, 40–49.
34. Feigon,J., Leupin,W., Denny,W.A. and Kearns,D.R. (1983) Two-dimensional proton nuclear magnetic-resonance investigation of the synthetic deoxyribonucleic-acid decamer $d(ATATCGATAT)_2$. *Biochemistry*, **22**, 5943–5951.
35. Scheek,R.M., Boelens,R., Russo,N., Van Boom,J.H. and Kaptein,R. (1984) Sequential resonance assignments in H-1-NMR spectra of oligonucleotides by two-dimensional NMR-spectroscopy. *Biochemistry*, **23**, 1371–1376.
36. Patel,D.J., Shapiro,L. and Hare,D. (1986) Sequence-dependent conformations of DNA duplexes—the TATA segment of the d(G-G-T-A-T-A-C-C) duplex in aqueous solution. *Biopolymers*, **25**, 693–706.
37. Wijmenga,S., Mooren,M.M. and Hilbers,C.W. (1993) NMR of nucleic acids; from spectrum to structure. In *NMR of nucleicacids; from spectrum to structure, A Practical Approach*. Oxford University Press, Oxford, pp. 218–288.
38. Wijmenga,S.S. and vanBuuren,B.N.M. (1998) The use of NMR methods for conformational studies of nucleic acids. *Prog. NMR Spec.*, **32**, 287–387.
39. Borgias,B.A. and James,T.L. (1990) MARDIGRAS—a procedure for matrix analysis of relaxation for discerning geometry of an aqueous structure. *J. Magn. Reson.*, **87**, 475–487.
40. Liu,H., Spielmann,H.P., Ulyanov,N.B., Wemmer,D.E. and James,T.L. (1995) Interproton distance bounds from 2D NOE intensities: effect of experimental noise and peak integration errors. *J. Biomol. NMR*, **6**, 390–402.

41. Tuma,J., Paulini,R., Rojas Stütz,J.A. and Richert,C. (2004) How much pi-stacking do DNA termini seek? Solution structure of a self-complementary DNA hexamer with trimethoxystilbenes capping the terminal base pairs. *Biochemistry*, **43**, 15680–15687.
42. Brünger,A.T., Adams,P.D., Clore,G.M., DeLano,W.L., Gros,P., Grosse-Kunstleve,R.W., Jiang,J.S., Kuszewski,J., Nilges,M., Pannu,N.S. *et al*. (1998) Crystallography and NMR system: a new software suite for macromolecular structure determination. *Acta Crystallogr. D Biol. Crystallogr*., **54**, 905–921.
43. Kleywegt,G.J. and Jones,T.A. (1997) Model building and refinement practice. *Methods Enzymol*., **277**, 208–230.
44. Stein,E.G., Rice,L.M. and Brünger,A.T. (1997) Torsion-angle molecular dynamics as a new efficient tool for NMR structure calculation. *J. Magn. Reson*., **124**, 154–164.
45. Ho,W.C., Steinbeck,C. and Richert,C. (1999) Solution structure of the aminoacyl-capped oligodeoxyribonucleotide duplex (W-TGCGCAC)$_2$. *Biochemistry*, **38**, 12597–12606.
46. Humphrey,W., Dalke,A. and Schulten,K. (1996) VMD: visual molecular dynamics. *J. Mol. Graph*., **14**, 33–38.
47. Kottysch,T., Ahlborn,C., Brotzel,F. and Richert,C. (2004) Stabilizing or destabilizing oligodeoxynucleotide duplexes containing single 2′-deoxyuridine residues with 5-alkynyl substituents. *Chemistry*, **10**, 4017–4028.
48. Bleczinski,C.F. and Richert,C. (1999) Steroid–DNA interactions increasing stability, sequence-selectivity, DNA/RNA discrimination, and hypochromicity of oligonucleotide duplexes. *J. Am. Chem. Soc*., **121**, 10889–10894.
49. Dogan,Z., Paulini,R., Rojas Stütz,J.A., Narayanan,S. and Richert,C. (2004) 5′-Tethered stilbene derivatives as fidelity- and affinity-enhancing modulators of DNA duplex stability. *J. Am. Chem. Soc*., **126**, 4762–4763.
50. Yan,N. (2004) Materials science. Nucleic acid nanotechnology. *Science*, **306**, 2048–2049.
51. Shen,Z., Yan,T., Wang,T. and Seeman,N.C. (2004) Paranemic crossover DNA: a generalized holliday structure with applications in nanotechnology. *J. Am. Chem. Soc*., **126**, 1666–1674.
52. SantaLucia,J. (1998) A unified view of polymer, dumbbell, and oligonucleotide DNA nearest-neighbor thermodynamics. *Proc. Natl Acad. Sci. USA*, **95**, 1460–1465.
53. Sandstrom,K., Warmlander,S., Leijon,M. and Graslund,A. (2003) $^1$H NMR studies of selective interactions of norfloxacin with double-stranded DNA. *Biochem. Biophys. Res. Commun*., **304**, 55–59.
54. Shen,L.L., Mitscher,L.A., Sharma,P.N., O'Donnell,T.J., Chu,D.W., Cooper,C.S., Rosen,T. and Pernet,A.G. (1989) Mechanism of inhibition of DNA gyrase by quinolone antibacterials: a cooperative drug-DNA binding model. *Biochemistry*, **28**, 3886–3894.